Refined Building Change Detection in Satellite Stereo Imagery Based on Belief Functions and Reliabilities

Jiaojiao Tian[1], Jean Dezert[2] and Peter Reinartz[1]

Abstract— Digital Surface Models (DSMs) generated from satellite stereo imagery provide valuable but not comprehensive information for building change detection. Therefore, belief functions have been introduced to solve this problem by fusing DSM information with changes extracted from images. However, miss-detection can not be avoided if the DSMs are containing large region of wrong height values. A refined workflow is thereby proposed by adopting the initial disparity map to generate a reliability map. This reliability map is then built in the fusion model. The reliability map has been tested in both Dempster-Shafer Theory (DST), and Dezert-Smarandache Theory (DSmT) frameworks. The results have been validated by comparing to the manually extracted change reference mask.

I. INTRODUCTION

In our previous research [1] [2], belief functions have performed very well for 3D building change detection. As we have mentioned, the accuracy of 2D change detection is limited due to the misdetections caused by irrelevant changes. These irrelevant changes have a larger effect on very high resolution (VHR) images since many details of building changes are expected. The DSMs generated from satellite stereo imagery can largely help to solve this problem. However, the DSMs may still exhibit some outliers resulting in occlusions within the stereo/multi views and due to matching mistakes. In this case, change information from spectral information of the original stereo imagery can and should be used together with height changes to eventually highlight building changes. For this purpose proper fusion theories and approaches are needed.

In paper [2], the belief functions introduced in the Dempster-Shafer Theory (DST) [3] [4], and extended in Dezert-Smarandache Theory (DSmT) [5] are used to deal with the uncertainty information delivered from the DSMs. In [2] the possibility of using Dempter's fusion rule and the Proportional Conflict Redistribution Rule #6 (PCR6) of DSmT in our application have been tested. Though improvements have been proven by comparing to the method stated in [1], false alarms can not be avoided in case of large regions of wrong height change values. Thereupon, in this paper the reliability map is adopted as an additional source of evidence to correct the basic Belief Assignments (BBAs) and thus refine the fusion model.

This paper is organized as follow. Firstly, the belief functions and building change detection fusion models are briefly reviewed. Then, the reliability discounting techniques are presented and the reliability map is generated. Later, the final four global BBAs are described together with the four decision criteria with which the final change detection mask can be generated. In the end, these refined fusion models are tested on two sets of satellite real data.

II. BELIEF FUNCTION BASED BUILDING CHANGE DETECTION

A. Basics of belief functions

Detailed presentations of DST and DSmT can be found in [5], [6] and [3]. Let Θ be a frame of discernment of a problem under consideration. $\Theta = \{\theta_1, \theta_2, \ldots, \theta_N\}$ consists of a list of N exhaustive and mutually exclusive elements θ_i, $i = 1, 2, \ldots, N$. Each θ_i represents a possible state related to the problem we want to solve. The assumption of exhaustivity and mutual exclusivity of elements of Θ is classically referred as *Shafer's model* of the frame Θ. A BBA also called a belief mass function (or just a mass for short), is a mapping $m(.) : 2^\Theta \to [0, 1]$ from the power set[1] of Θ denoted 2^Θ to $[0, 1]$, that verifies [3]:

$$m(\emptyset) = 0 \quad \text{and} \quad \sum_{X \in 2^\Theta} m(X) = 1. \quad (1)$$

$m(X)$ represents the mass of belief exactly committed to X. An element $X \in 2^\Theta$ is called a focal element if and only if $m(X) > 0$. In DST, the combination (fusion) of several independent sources of evidences is done with Dempster-Shafer[2] (DS) rule of combination, assuming that the sources are not in total conflict[3]. DS combination of two independent BBAs $m_1(.)$ and $m_2(.)$, denoted symbolically by $DS(m_1, m_2)$, is defined by $m^{DS}(\emptyset) = 0$, and for all $X \in 2^\Theta \setminus \{\emptyset\}$ by:

$$m^{DS}(X) = \frac{1}{1 - K^{DS}} \sum_{\substack{X_1, X_2 \in 2^\Theta \\ X_1 \cap X_2 = X}} m_1(X_1) m_2(X_2), \quad (2)$$

where the total degree of conflict K^{DS} is given by

$$K^{DS} \triangleq \sum_{\substack{X_1, X_2 \in 2^\Theta \\ X_1 \cap X_2 = \emptyset}} m_1(X_1) m_2(X_2). \quad (3)$$

---

[1]The power set is the set of all subsets of Θ, empty set included.

[2]Although the rule has been proposed originally by Dempster, we call it Dempster-Shafer rule because it has been widely promoted by Shafer in DST.

[3]otherwise DS rule is mathematically not defined because of 0/0 indeterminacy.

[1]Jiaojiao Tian and Peter Reinartz are with Remote Sensing Technology Institute, German Aerospace Center, 82234 Oberpfaffenhofen, Germany jiaojiao.tian@dlr.de, peter.reinartz@dlr.de

[2]Jean Dezert with the The French Aerospace Lab, Chemin de la Hunière, Palaiseau, F-91761, France jean.dezert@onera.fr

A discussion on the validity of DS rule and its incompatibility with Bayes fusion rule for combining Bayesian BBAs can be found in [6], [7], [8]. To circumvent the problems of DS rule, Smarandache and Dezert (see [5], Vol. 2, Chap. 1), then Martin and Osswald (see [5], Vol. 2, Chap. 2) have developed in DSmT [5] two fusion rules called PCR5 and PCR6 based on the proportional conflict redistribution (PCR) principle which consists

1) to apply the conjunctive rule;
2) calculate the total or partial conflicting masses;
3) then redistribute the (total or partial) conflicting mass proportionally on non-empty sets according to the integrity constraints one has for the frame Θ.

This PCR principle transfers the conflicting mass only to the elements involved in the conflict and proportionally to their individual masses, so that the specificity of the information is not degraded. Because the proportional transfer can be done in two different ways, this has yielded to two different fusion rules. It has been proved in [9] that only PCR6 rule is compatible with frequentest probability estimation, and that is why we recommend its use in the applications. PCR5 and PCR6 rules simplify greatly and coincide for the combination of two sources. In this case, the PCR6 combination is obtained by taking $m^{PCR6}(\emptyset) = 0$, and for all $X \neq \emptyset$ in 2^Θ by

$$m^{PCR6}(X) = \sum_{\substack{X_1, X_2 \in 2^\Theta \\ X_1 \cap X_2 = X}} m_1(X_1)m_2(X_2) +$$
$$\sum_{\substack{Y \in 2^\Theta \setminus \{X\} \\ X \cap Y = \emptyset}} [\frac{m_1(X)^2 m_2(Y)}{m_1(X) + m_2(Y)} + \frac{m_2(X)^2 m_1(Y)}{m_2(X) + m_1(Y)}], \quad (4)$$

where all denominators in Eq. (4) are different from zero. If a denominator is zero, that fraction is discarded. If a denominator, e.g., $m_1(X) + m_2(Y)$ tends towards 0, then also the conflicting mass $m_1(X)m_2(Y)$ that is transferable tends to zero because $m_1(X)$ and $m_2(Y)$ tend to zero (since they are positive), therefore the redistribution masses also tend to zero. That reflects the continuity of PCR6.

B. BBAs for Building change detection

1) Choice of the frame of discernment: Focusing on building change detection, two change indicators, one from images and one from DSMs are used. Changes from spectral images are highlighted by using the Iteratively Reweighted Multivariate Alteration Detection (IRMAD) [10]. Consequently height changes from DSMs are shown after robust height difference [1]. Three classes are considered to define the frame of discernment satisfying Shafer's model:

$$\Theta = \{\theta_1 \triangleq \text{Pixel} \in \text{BuildingChange},$$
$$\theta_2 \triangleq \text{Pixel} \in \text{OtherChange}, \quad (5)$$
$$\theta_3 \triangleq \text{Pixel} \in \text{NoChange}\},$$

and

$$\theta_1 \cap \theta_2 \cap \theta_3 = \varnothing. \quad (6)$$

Based on the three classes, the set of focal elements FE that are of interest in our application is:

$$FE = \{\theta_1, \theta_2, \theta_3, \theta_1 \cup \theta_2, \theta_2 \cup \theta_3, \theta_1 \cup \theta_2 \cup \theta_3\}. \quad (7)$$

2) BBAs construction: Paper [2] constructed the sigmoidal model for both concordance and discordance indexes. The details and advantages of this approach are described in [11]. The concordance index measures the concordace of change indicator and BBA in the assertion, while the discordance measures the opposition of change indicator to the BBAs in the assertion. The original sigmoid curve is defined as

$$f_{(\tau,T)}(x) = 0.99/(1 + e^{-\frac{x-T}{\tau}}), \quad (8)$$

where x is the original value of each indicator. Two parameters T and τ are used to control the symmetry point and the slope of the sigmoid function. The symmetry point indicates a certainty of 50%. In [11] these two parameters T and τ are manually given. Here, the multi-level Otsu's thresholding method [12] is used for automatically getting the symmetry points for both concordance index and discordance index. Otsu's algorithm defines that an image is composed of objects and background. A discriminant analysis is performed by minimizing the intra-class variance. When three classes are of interest, two threshold values are expected. Otsu's method can be extended to

$$\sigma_\omega^2(T_1, T_2) = \omega_1 \sigma_1^2(T_1, T_2)$$
$$+ \omega_2 \sigma_2^2(T_1, T_2) + \omega_3 \sigma_3^2(T_1, T_2). \quad (9)$$

The weights ω_i are the probabilities obtained from the image histogram that are separated by the thresholds T_1 and T_2. σ_i is the standard deviation of the i-th class, for $i = 1, 2, 3$. T_1 and T_2 can be used as the symmetry points of discordance and concordance index respectively. Thus, using height change index as example, the BBAs for discordance and concordance height change index are functions of values $a_{\Delta H}$ and $b_{\Delta H}$ defined by

$$a_{\Delta H} = f_{\tau, T_1}(\Delta H), \quad \text{and} \quad b_{\Delta H} = f_{-\tau, T_2}(\Delta H). \quad (10)$$

The factor τ is calculated with a sample value ($\Delta H = 1$, $a_{\Delta H} = 0.1$), which means 1 meter height change indicates 10% probability to be building changes. The BBAs for discordance and concordance image change index are built similarly. Differences appearing in 2D images give a concordance indication for all changes, which include the building changes and other changes ($\theta_1 \cup \theta_2$). In this paper the changes from images are named ΔImg.

In the Tables I and II, we present the two ways of construction of the BBAs from the sources of evidence based either on DS or on PCR6 rules of combination for the height change indicator (i.e. the first source of evidence) and the image change indicator (i.e. the second source of evidence). In Table I, $m_1(.)$ and $m_1'(.)$ represent the concordance and discordance BBAs from ΔH, whereas in Table II $m_2(.)$ and $m_2'(.)$ represent the concordance and discordance BBAs from images.

TABLE I

BBA CONSTRUCTION FOR HEIGHT CHANGE INDICATOR ΔH. $[K_{\Delta H} = a_{\Delta H}b_{\Delta H}]$

Focal Elem.	$m_1(.)$	$m_1'(.)$	$m_1^{DS}(.)$	$m_1^{PCR6}(.)$
θ_1	$a_{\Delta H}$	0	$\frac{a_{\Delta H}(1-b_{\Delta H})}{1-K_{\Delta H}}$	$a_{\Delta H}(1-b_{\Delta H}) + \frac{a_{\Delta H}K_{\Delta H}}{a_{\Delta H}+b_{\Delta H}}$
θ_2	0	0	0	0
θ_3	0	0	0	0
$\theta_1 \cup \theta_2$	0	0	0	0
$\theta_2 \cup \theta_3$	0	$b_{\Delta H}$	$\frac{(1-a_{\Delta H})b_{\Delta H}}{1-K_{\Delta H}}$	$(1-a_{\Delta H})b_{\Delta H} + \frac{b_{\Delta H}K_{\Delta H}}{a_{\Delta H}+b_{\Delta H}}$
$\theta_1 \cup \theta_2 \cup \theta_3$	$1-a_{\Delta H}$	$1-b_{\Delta H}$	$\frac{(1-a_{\Delta H})(1-b_{\Delta H})}{1-K_{\Delta H}}$	$(1-a_{\Delta H})(1-b_{\Delta H})$

TABLE II

BBA CONSTRUCTION FOR IMAGE CHANGE INDICATOR ΔImg. $[K_{\Delta Img} = a_{\Delta Img}b_{\Delta Img}]$

Focal Elem.	$m_2(.)$	$m_2'(.)$	$m_2^{DS}(.)$	$m_2^{PCR6}(.)$
θ_1	0	0	0	0
θ_2	0	0	0	0
θ_3	0	$b_{\Delta Img}$	$\frac{(1-a_{\Delta Img})b_{\Delta Img}}{1-K_{\Delta Img}}$	$(1-a_{\Delta Img})b_{\Delta Img} + \frac{b_{\Delta Img}K_{\Delta Img}}{a_{\Delta Img}+b_{\Delta Img}}$
$\theta_1 \cup \theta_2$	$a_{\Delta Img}$	0	$\frac{a_{\Delta Img}(1-b_{\Delta Img})}{1-K_{\Delta Img}}$	$a_{\Delta Img}(1-b_{\Delta Img}) + \frac{a_{\Delta Img}K_{\Delta Img}}{a_{\Delta Img}+b_{\Delta Img}}$
$\theta_2 \cup \theta_3$	0	0	0	0
$\theta_1 \cup \theta_2 \cup \theta_3$	$1-a_{\Delta Img}$	$1-b_{\Delta Img}$	$\frac{(1-a_{\Delta Img})(1-b_{\Delta Img})}{1-K_{\Delta Img}}$	$(1-a_{\Delta Img})(1-b_{\Delta Img})$

III. RELIABILITY DISCOUNTING

The reliability discounting has been described and discussed in the references [13] and [14]. Briefly said, if an additional knowledge about the reliability (α) of certain indicator (X) is available, it can be adopted to refine the initial BBAs. α would be a value ranging from 0 to 1. And $\alpha = 1$ means fully reliable, while $\alpha = 0$ means the indicator is totally unreliable. Based on Shafer's discounting model [3], the reliability discounting factor α is introduced to discount any BBA $m(.)$ defined on the power set 2^Θ as follows:

$$\begin{cases} m_\alpha(X) = \alpha \cdot m(X), \text{for } X \neq \Theta \\ m_\alpha(\Theta) = \alpha \cdot m(\Theta) + (1-\alpha). \end{cases} \quad (11)$$

In the DSM assisted building change detection, false alarms are detected if wrong heights are present in DSM for large regions [1]. And these wrong heights are mostly introduced not in the stereoscope images matching procedure, but in the gaps filling step. In our DSM generation procedure, the height of un-matched pixels are interpolated using the height values of neighborhood pixels. Therefore, a reliable height value can be achieved for small gaps. When large gaps turn up in the disparity map, for example, a whole building roof, the height of that building can not be correctly interpolated. Thus, the percentage of available correctly matched neighborhood pixels inside a predefined region can be used to generate the height reliability. Fig. 1 shows an example of the generated reliability map. Fig. 1a is the gaps mask. The gaps region of the disparity map is represented with black color. Pixels with proper elevation values are displayed with white color. It can be observed, based on our approach that pixels in the center of a gap get lower reliability factor values than pixels next to the gap boundary (see Fig.1b). In the building
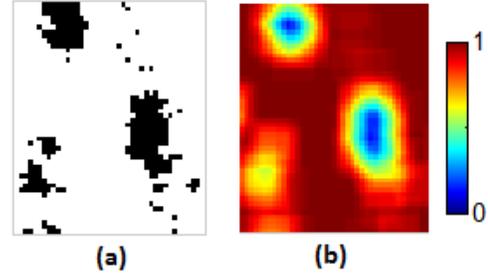
Fig. 1.   Reliability map (b) generated from the gaps mask (a).

change detection procedure, the reliability map of two DSMs (α_{DSM1} and α_{DSM2}) are calculated respectively. They are then fused together to generate a final reliability map $\alpha_{\Delta H}$ for the height change indicator.

$$\alpha_{\Delta H} = \alpha_{DSM1} \cdot \alpha_{DSM2}. \quad (12)$$

IV. GLOBAL BBAS AND CHANGE DETECTION

A. Global BBAs generation

The BBAs related with the concordance and discordance indexes are combined to get the global BBA regarding to each source of evidence. These global BBAs will then be used as input for solving the change detection problem thanks to their combination. From the previous step of BBAs modelings, each pixel will get two sets of BBAs to combine results from Table I and II. More precisely, we will have to combine either $\{m_1^{DS}(.), m_2^{DS}(.)\}$ if DS rule is preferred for the BBA modeling, or $\{m_1^{PCR6}(.), m_2^{PCR6}(.)\}$ if the PCR6 rule is adopted. These BBAs from Table I and II have been represented by a_1, b_1, c_1 and a_2, b_2, c_2. In this paper, the mass values a_1, b_1, and c_1 are further discounted by the generated

reliability map $\alpha_{\Delta H}$ and denoted respectively as A_1, B_1, and C_1. More precisely, one computes

$$\begin{cases} A_1 = \alpha_{\Delta H} \cdot a_1 \\ B_1 = \alpha_{\Delta H} \cdot b_1 \\ C_1 = \alpha_{\Delta H} \cdot c_1 + (1 - \alpha_{\Delta H}). \end{cases} \quad (13)$$

In this application, only the reliability map for height change indicators is generated. The reliability map for image change indicators can also be constructed according to the change objects of interested. For instance, vegetation mask can be used to discount the reliability of building changes. However, this paper focuses on the reliability of height information. When the reliability map of image changes is available, it could be used as the same way as height change reliability map. Table III and Table IV describe the final building change detection models based either on DS or on PCR6 rules. Here, the discounted height change indicators is denoted as $m_{1\alpha_{\Delta H}}(.)$.

TABLE III

DS FUSION MODEL FOR BUILDING CHANGE DETECTION.

Focal Elem.	$m_{1\alpha_{\Delta H}}(.)$	$m_2(.)$	$m_{12}^{DS}(.)$
θ_1	A_1	0	$\frac{A_1(b_1+b_3)}{1-A_1b_2}$
θ_2	0	0	$\frac{A_2b_1}{1-A_1b_2}$
θ_3	0	b_2	$\frac{(A_2+a_3)b_2}{1-A_1b_2}$
$\theta_1 \cup \theta_2$	0	b_1	$\frac{A_3b_1}{1-A_1b_2}$
$\theta_2 \cup \theta_3$	A_2	0	$\frac{A_2b_3}{1-A_1b_2}$
Θ	A_3	b_3	$\frac{A_3b_3}{1-A_1b_2}$

TABLE IV

PCR6 FUSION MODEL FOR BUILDING CHANGE DETECTION.

Focal Elem.	$m_{1\alpha_{\Delta H}}(.)$	$m_2(.)$	$m_{12}^{PCR6}(.)$
θ_1	A_1	0	$A_1(b_1+b_3) + \frac{A_1A_1b_2}{A_1+b_2}$
θ_2	0	0	A_2b_1
θ_3	0	b_2	$(A_2+a_3)b_2 + \frac{b_2A_1b_2}{A_1+b_2}$
$\theta_1 \cup \theta_2$	0	b_1	A_3b_1
$\theta_2 \cup \theta_3$	A_2	0	A_2b_3
Θ	A_3	b_3	A_3b_3

$m_{1\alpha_{\Delta H}}(.)$ can be obtained from the discounting of the fusion results presented in Table I. Thus they have been denoted respectively as $m_{1\alpha_{\Delta H}}^{DS}(.)$ and $m_{1\alpha_{\Delta H}}^{PCR6}(.)$. This discounted height change indicators are fused in the second step with image change indicator $m_2(.)$ to generate the final global BBAs. From the tables III and IV, four sets of global BBAs can be computed based on different BBAs and fusion methods as follows:

$$\begin{aligned} G_1 &= DS\{m_{1\alpha_{\Delta H}}^{DS}(.), m_2^{DS}(.)\} \\ G_2 &= PCR6\{m_{1\alpha_{\Delta H}}^{DS}(.), m_2^{DS}(.)\} \\ G_3 &= DS\{m_{1\alpha_{\Delta H}}^{PCR6}(.), m_2^{PCR6}(.)\} \\ G_4 &= PCR6\{m_{1\alpha_{\Delta H}}^{PCR6}(.), m_2^{PCR6}(.)\}. \end{aligned} \quad (14)$$

For example, if both the BBA modeling procedure and global BBAs are constructed based on DS fusion rule, the generated global BBA is recorded as G_1.

B. Change mask generation

After the fusion step, each pixel in the images will get a certain degree of belief for all focal elements. The value of global BBAs in θ_1 gives a direct building change probability map. A change mask can be generated after giving a threshold value. However, BBAs on the partial ignorance and full ignorance set should also be considered in the decision making procedure. DST and DSmT propose different approaches to take the final decision. In this work, the same decision criteria as used in [2] are tested. They are: 1) maximum of global BBAs (Max_Bel), 2) maximum of plausibility (Max_Pl), 3) maximum of betting probabilities (Max_BetP) and 4) the maximum of DSmP (Max_DSmP). The reader can refer to [3] and [5] (Vol. 3, Chap. 3) for the mathematical definitions of $Bel(.)$, $Pl(.)$, $BetP(.)$ and $DSmP(.)$ functions.

V. EXPERIMENTS

The improved building change detection fusion models have been tested on satellite images. The datasets and the experiments are described in this section.

A. Datasets

The experimental datasets consist of two pairs of IKONOS stereo imagery captured in February 2006 and May 2011 respectively shown in Fig. 2 and 3. The first two images in each figure are the panchromatic images of two dates. (c) and (d) are the generated DSMs. They have been generated based on the method explained in [15]. The colors represent the height range in this test region.
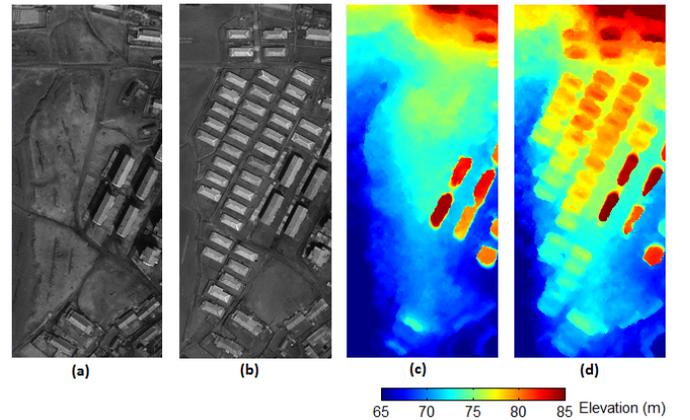
Fig. 2. Experimental dataset: a) panchromatic image from date1; b) panchromatic image from date2; c) DSM from date1; d) DSM from date2.

The spatial co-registration is achieved though camera model parameter corrections before the DSM generation procedure [15]. The radiometrical co-registration method has been described in [1]. Fig. 2 shows a normal building change example. Several buildings have been built on flat surface. The generated DSMs are displayed in Fig. 2c and d. In the second example (shown in Fig. 3), a large percentage of pixels on the roof of the large building in the center appear as gaps in the disparity map. In the filling procedure, the
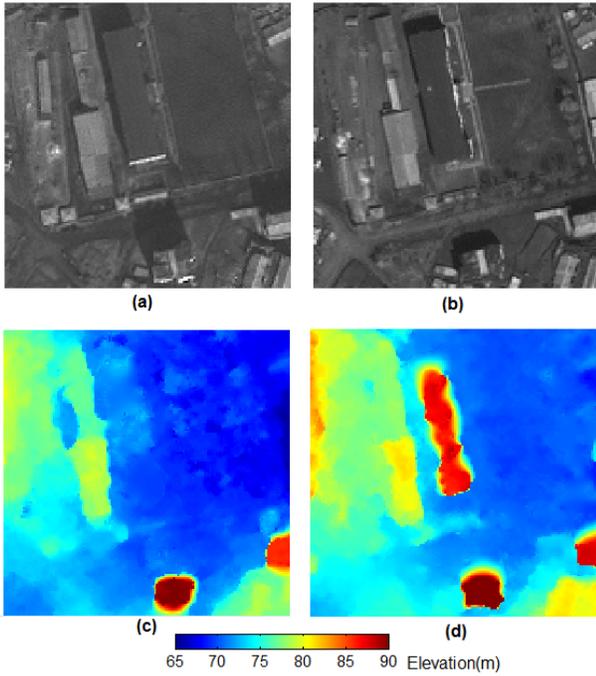
Fig. 3. Datasets of the 2nd test region; a) panchromatic image from date1; b) panchromatic image from date2; c) DSM from date1; (d) DSM from date2.

large size of the gap in the date1 data lead to the missing of this building in the DSM (Fig. 3c).

B. Results and evaluation

The refined DS fusion model and PCR6 fusion model have been applied to both datasets respectively. To show the improvement obtained by our method, we have compared its results with the original results we can obtain with the method in [2]. Firstly, the global BBAs of θ_1 are compared and displayed in Fig. 4 below.
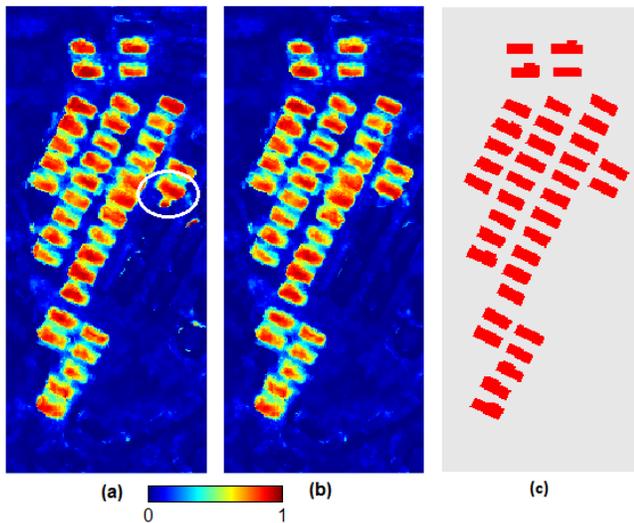
Fig. 4. Global Building change BBAs (a) Initial result; (b) Refined result; (c) Ground truth.

Fig. 4(a) corresponds to the original[4] result, and Fig. 4(b) shows the refined result based on $G_1(\theta_1)$. By comparing to the ground truth (Fig. 4(c)), the improvements can be clearly observed in the building boundary regions, especially the building marked with a white circle. In the initial result, the pixels next to this building are falsely detected as BuildingChange.

To evaluate quantitatively the performances of the different fusion approaches, the extracted BBAs from both approaches (original and refined) are compared to the manually extracted change reference masks. The results are analyzed in terms of Receiver Operating Characteristic (ROC) curve [16]. A larger area under the ROC curve (AUC) indicates a better accuracy of the building change map. The numerical evaluation results are described in Table V. The obtained AUC values prove a general improvement after reliability discounting is applied.

TABLE V
QUALITY COMPARISON OF GLOBAL BBA (BUILDING CHANGE).

	Test Region 1		Test Region 2	
	Original	Refined	Original	Refined
G_1	0.9811	0.9833	0.9509	0.9950
G_2	0.9829	0.9839	0.9485	0.9931
G_3	0.9815	0.9837	0.9512	0.9955
G_4	0.9835	0.9844	0.9487	0.9939

In addition to the AUC comparison, the building change masks extracted from these four global BBAs sets are compared and evaluated. Each global BBA set can generate four building change masks based on these four decision criteria. These building change masks are compared with the masks from paper [2] based on Kappa statistic (KA). The comparison results of Test region 1 are shown in Table VI. Limited by the reference data we can get, only the building change frame is evaluated here. One sees the reliability discounting map helps to improve the result accuracy in all fusion and decision approaches.

In the second test region, there is actually no building changes. The purpose of showing this test region is to further prove the advantage of the extracted reliability map. Fig. 5 shows the extracted reliability discounting map of the height changes. The windowsize we selected for this test region is 9×9. By using this reliability map, final fusion result of $G_1(\theta_1)$ is achieved and shown in Fig. 6(a). As a comparison, the $G_1(\theta_1)$ of the initial fusion model is displayed in Fig. 6(b). This is the same building that we have discussed in paper [1]. It can be noted in Fig. 3, this building exists in both panchromatic images of two dates. However, only the DSM from date1 contains the correct height of this building. In Fig. 3c, this building can not be recognized. Therefore, a very high BBA would be achieved in the height change indicator. A high value in $m_1(.)$ leads to a high global BBAs in building changes (as shown in Fig. 6(a)). Thus this building would be falsely detected as building changes. However, after discounting this region has much lower global BBAs (see Fig. 6(b)), and can be further correctly detected as NoChange.

[4]obtained without reliability discounting, as presented in [2].

TABLE VI

CHANGE MASKS EVALUATION FROM FOUR GLOBAL BBAs.

	G_1		G_2		G_3		G_4	
	Original	Refined	Original	Refined	Original	Refined	Original	Refined
Max_Bel	0.9271	0.9324	0.9271	0.9324	0.9266	0.9322	0.9265	0.9321
Max_Pl	0.9291	0.9342	0.9288	0.9339	0.9287	0.9339	0.9284	0.9336
Max_BetP	0.9283	0.9335	0.9282	0.9334	0.9279	0.9333	0.9278	0.9333
Max_DSmP	0.9281	0.9333	0.9280	0.9331	0.9278	0.9331	0.9276	0.9330
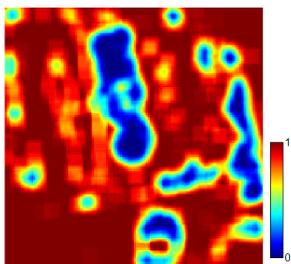
Fig. 5. Generated height change reliability map of the test region 2.
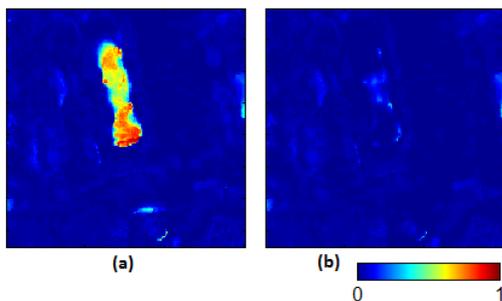
Fig. 6. Global Building change BBAs (a) Initial result; (b) Refined result.

VI. CONCLUSIONS

Building change detection is a difficult topic, especially when the building changes happen together with other irrelevant changes. Our previous research has evidenced the performance of the belief functions in DSM assisted change detection [2]. In this paper, the change detection accuracy is further improved by adopting an additional reliability map. Height has proved to be an important feature for building change detection. However, the DSMs from satellite images do not always provide reliable height information, due to the occlusion and matching errors. The wrong height information will thus bring false alarms to the change detection procedure. Therefore, the original unfilled disparity maps are adopted to generate an height change reliability map, which is further used in the fusion models.

Our first experimental results have shown that this reliability map can improve the quality of all four global BBAs, and further influences the final change detection results from four decision criteria. However, the two test regions were quite small to draw a definitive conclusion that is why more experiments will be performed on a wider variety of regions with different types of backgrounds. A detailed statistical analysis and comparisons of the results with other techniques is under progress and they will be presented in a forthcoming publication.

Generally speaking, both DST and DSmT frameworks offer the possibility to reach a high accuracy result. The workflow proposed in this paper enables an automatic building change detection procedure. Other reliability maps from images would be further adopted in future work. Furthermore, besides building changes, more change objects will be considered in the fusion model.

REFERENCES

[1] J. Tian, S. Cui, and P. Reinartz, "Building change detection based on satellite stereo imagery and digital surface models," *IEEE Trans. Geosci. Remote Sens.*, vol. 52, no. 1, pp. 406–417, 2014.
[2] J. Tian, P. Reinartz, and J. Dezert, "Building change detection in satellite stereo imagery based on belief functions," in *Urban Remote Sensing Event (JURSE), 2015 Joint*. IEEE, 2015, pp. 1–4.
[3] G. Shafer, *A mathematical theory of evidence*. Princeton university press Princeton, 1976.
[4] A. Dempster, "Upper and lower probabilities induced by a multivalued mapping," *The Annals of Mathematical Statistics*, vol. 38, no. 2, pp. 325–339, 1967.
[5] F. Smarandache and J. Dezert, *Advances and Applications of DSmT for Information Fusion*. American Research Press, Rehoboth, NM, U.S.A, 2004–2015, vol. 1–4. [Online]. Available: http://www.onera.fr/staff/jean-dezert?page=2
[6] J. Dezert and A. Tchamova, "On the validity of Dempster's fusion rule and its interpretation as a generalization of bayesian fusion rule," *Int. J. Intell. Syst.*, vol. 29, no. 3, pp. 223–252, 2014.
[7] J. Dezert, P. Wang, and A. Tchamova, "On the validity of Dempster-Shafer theory," in *Proc. of FUSION 2012*, 2012, pp. 655–660. [Online]. Available: http://fs.gallup.unm.edu//DSmT.htm
[8] A. Tchamova and J. Dezert, "On the behavior of Dempster's rule of combination and the foundations of dempster-shafer theory," in *Proc. of IS 2012*, 2012, pp. 108–113.
[9] F. Smarandache and J. Dezert, "On the consistency of PCR6 with the averaging rule and its application to probability estimation," in *Proc. of FUSION 2013*, 2013, pp. 1119–1126.
[10] A. A. Nielsen, "The regularized iteratively reweighted MAD method for change detection in multi-and hyperspectral data," *IEEE Trans. Image Process.*, vol. 16, no. 2, pp. 463–478, 2007.
[11] J. Dezert and J.-M. Tacnet, "Sigmoidal model for belief function-based Electre Tri method," in *Belief Functions: Theory and Applications*, 2012, pp. 401–408.
[12] N. Otsu, "A threshold selection method from gray-level histograms," *IEEE Trans. Syst., Man, Cybern.*, vol. 9, no. 1, pp. 62–66, 1975.
[13] D. Mercier, B. Quost, and T. Denœux, "Contextual discounting of belief functions," in *Symbolic and Quantitative Approaches to Reasoning with Uncertainty*. Springer, 2005, pp. 552–562.
[14] F. Smarandache, J. Dezert, and J.-M. Tacnet, "Fusion of sources of evidence with different importances and reliabilities," in *Proc. of FUSION2010*. IEEE, 2010, pp. 1–8.
[15] P. dAngelo and P. Reinartz, "DSM based orientation of large stereo satellite image blocks," *Int. Arch. Photogramm. Remote Sens. Spatial Inf. Sci*, vol. 39, no. B1, pp. 209–214, 2012.
[16] M. H. Zweig and G. Campbell, "Receiver-operating characteristic (ROC) plots: a fundamental evaluation tool in clinical medicine." *Clinical chemistry*, vol. 39, no. 4, pp. 561–577, 1993.